Electronic Supplementary Material (ESI) for New Journal of Chemistry.

A multifunctional fluorescent probe of Cd-MOF, synthesis, structure, and its sensing properties

Lu Liu, Yuejiao Jia, Dechao Li, Chen Chen, Ming Hu*[1]

[1]Inner Mongolia Key Laboratory of Chemistry and Physics of Rare Earth Materials; School of Chemistry and Chemical Engineering, Inner Mongolia University, Hohhot 010021, China. Tel.: +86-471-4992981. *E-mail addresses*: hm988@126.com.

Supporting Information

Materials and general methods

All chemicals were commercially obtained that without further purification. $Eu(NO_3)_3 \cdot 6H_2O$ and H_2bpdc were purchased by Jinan Henghua Sci. & Tec. Co., Ltd. Elemental analyses (C, H and N) were measured on a PerkinElmer 2400 analyzer. The IR spectra were understaned using KBr pellets on a Nicolet Avatar-360 spectrometer in the 400–4000 cm−1 region. Thermogravimetric analyses (TGA) were recorded on a PerkinElmer TG-7 analyzer heated from 30 to 1000℃ under a nitrogen atmosphere. Powder X-ray diffraction (PXRD) was performed on an Analytical Empyrean instrument using Cu Kα radiation at room temperature. The Photoluminescence (PL) spectra were measured on a FLS920 spectrophotometer. The UV–vis spectroscopic researches were received on a Hitachi U-3900 spectro-photometer. X-ray photoelectron spectroscopy(XPS) were studies on a Thermo Scientific ESCALAB 250Xi photo-electron spectrometer.

X-Ray crystallography

Crystallographic data for **1** and **2** was collected on a Bruker Smart 1000 diffractometer equipped with graphite-monochromatic Cu Kα radiation ($\lambda = 0.71073$ Å) using the ω-scan technique at room temperature. Semiempirical absorption corrections were applied using the SADABS program. The structure was solved by direct methods using SHELXS-2018 and was refined by full matrix least-squares on $|F|^2$ using the SHELXTL-2018 program. All non-hydrogen atoms were refined anisotropically. The organic hydrogen atoms were geometrically generated, the hydrogen atoms of water molecules were located from difference Fourier maps and were refined with the common isotropic thermal parameter. Details of the crystal parameter data collection and refinement for **1** are summarized in Supplementary Table S1.

Luminescence sensing experiments

In a typical fluorescence sensing experiment of complex **1**, 1.65 mg of ground compound **1** was dispersed in 3.0 mL deionized water. After adding different analytes,

the uniform suspension was formed after ultrasonic treatment at room temperature for 30 min. The suspension was added into the quartz tube and the fluorescence spectrum was measured at 356 nm excited and a slit width of 2 nm.

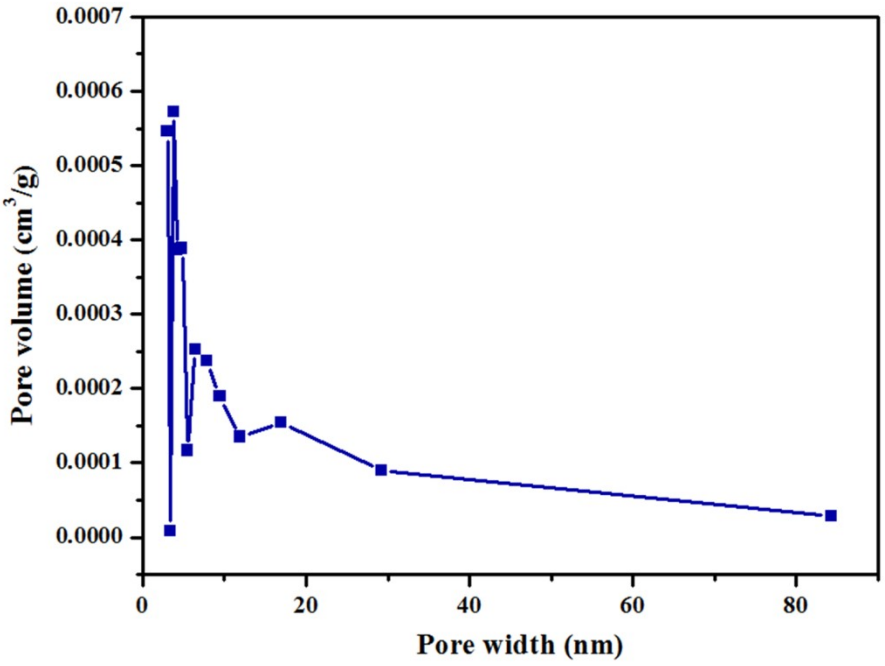

Fig.S1 The BJH pore diameter distribution curve.

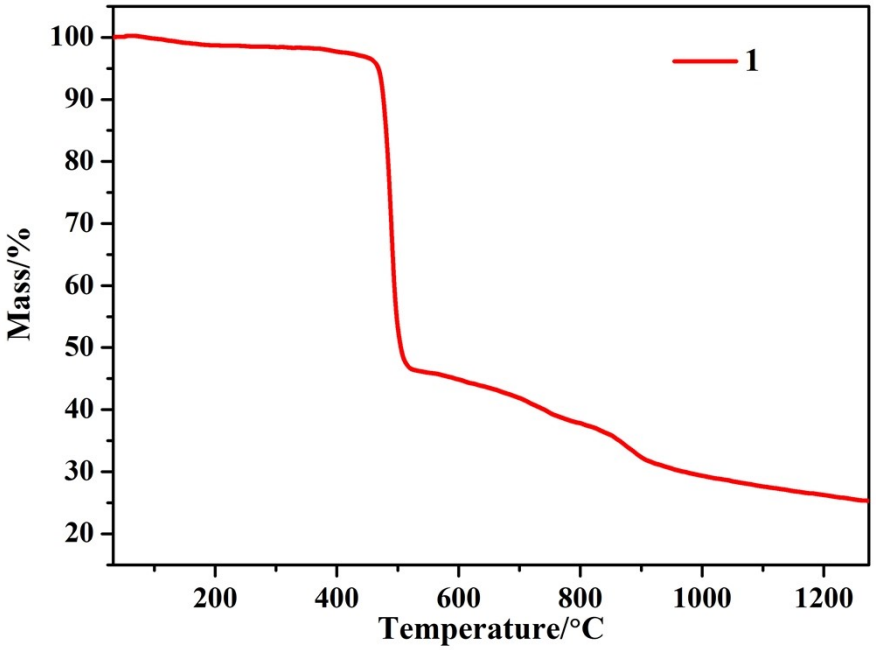

Fig.S2 TG analysis plots of complex **1**.

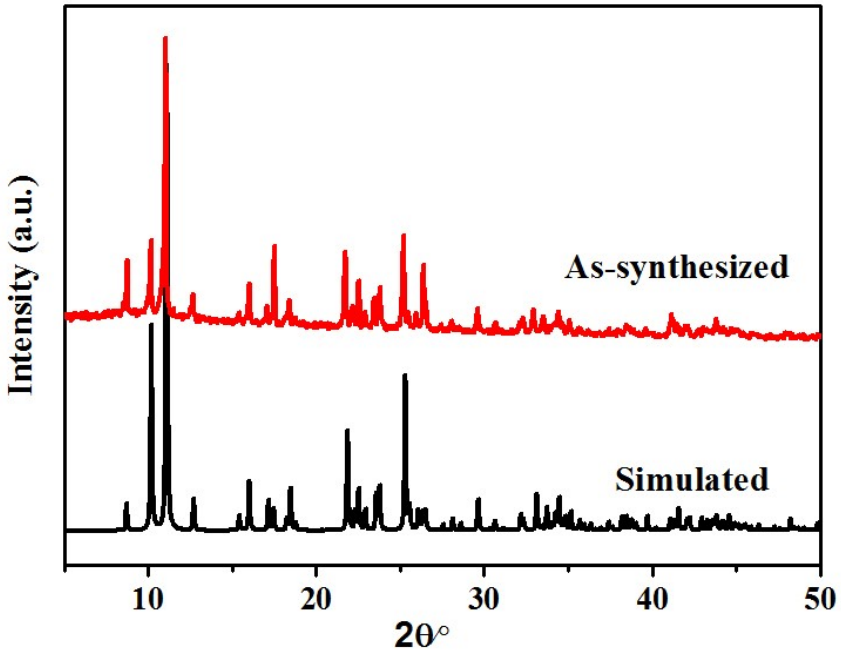

Fig.S3 PXRD Patterns of complex **1** simulated from the X-ray single-crystal structure and as- synthesized samples of complex **1**.

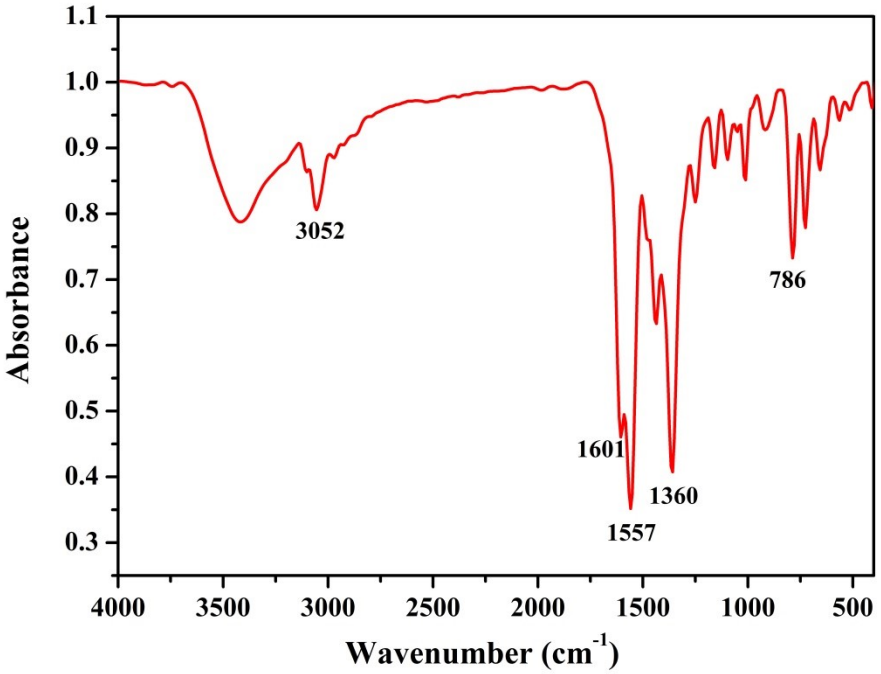

Fig.S4 IR spectra of complex **1**.

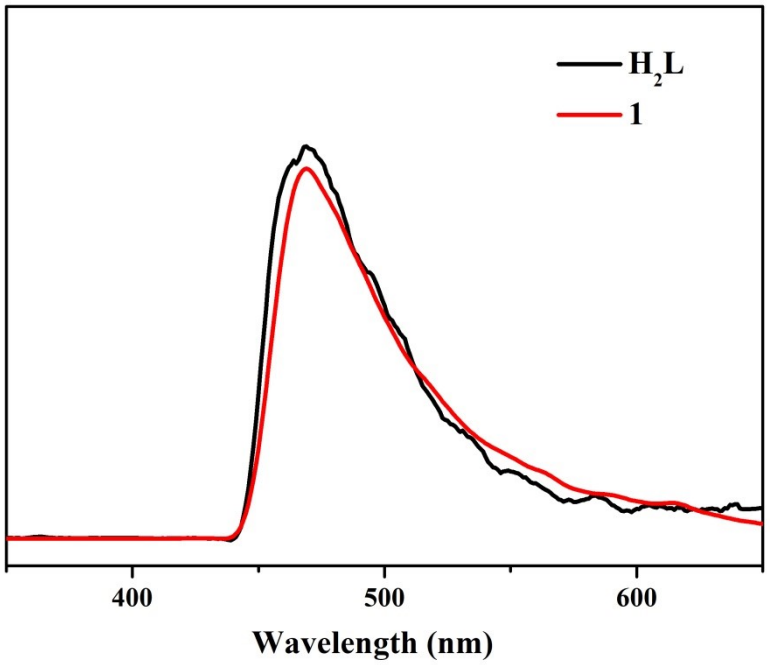

Fig.S5 The emission spectra of H_2dbta and complex **1** at room temperature.

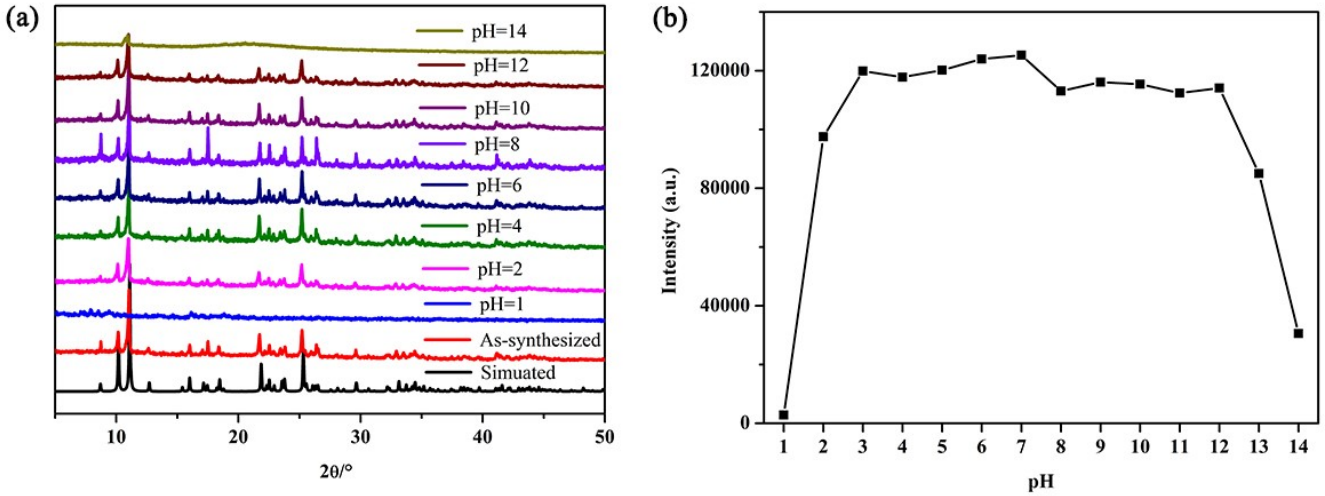

Fig.S6 (a) PXRD patterns of complex **1** dispersed in aqueous solutions of pH = 1-14; (b) Comparison of intensity of complex **1** in aqueous solutions of pH = 1-14 when excited at 356 nm.

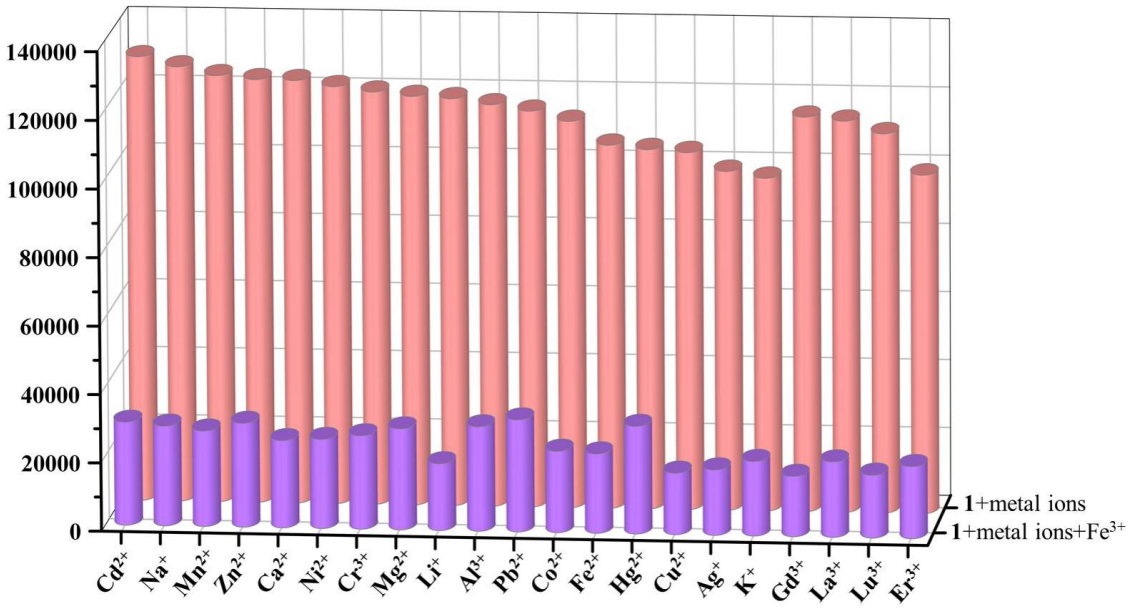

Fig.S7 The anti-interference experiment of complex **1** for detecting Fe^{3+} ions in the presence of other cations (1.0×10^{-3} M).

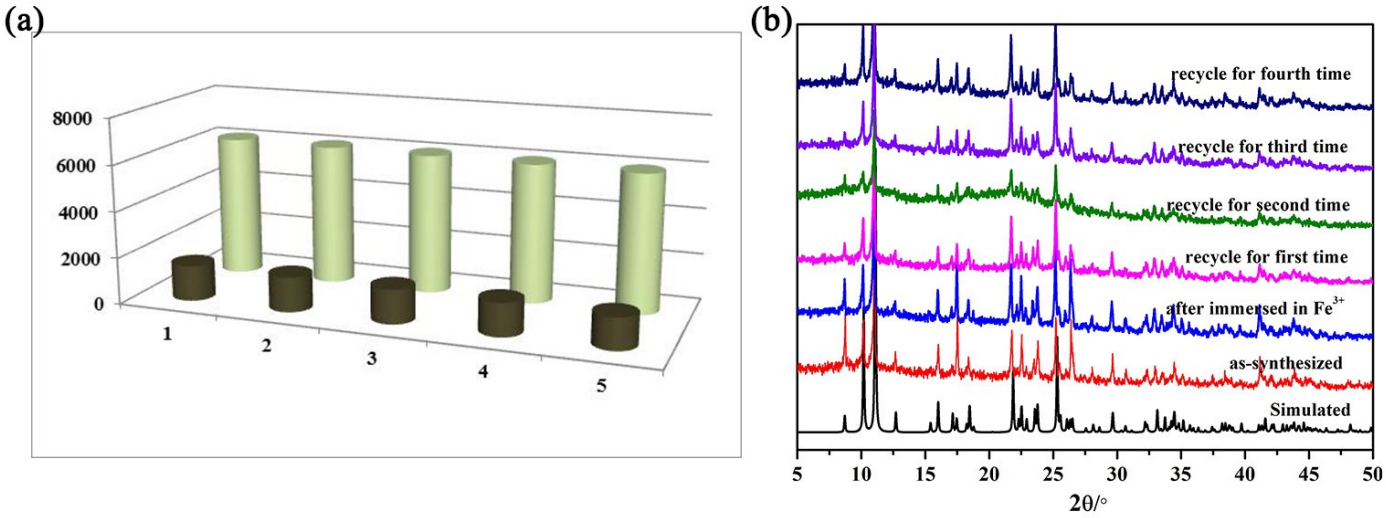

Fig.S8 (a) Recovery experiment of Fe^{3+} detected by complex **1**: the light colored cylindrical bar represents the initial luminous intensity, and the dark colored cylindrical bar represents the luminous intensity after adding Fe^{3+} ions; (b) PXRD patterns complex **1** after cycling.

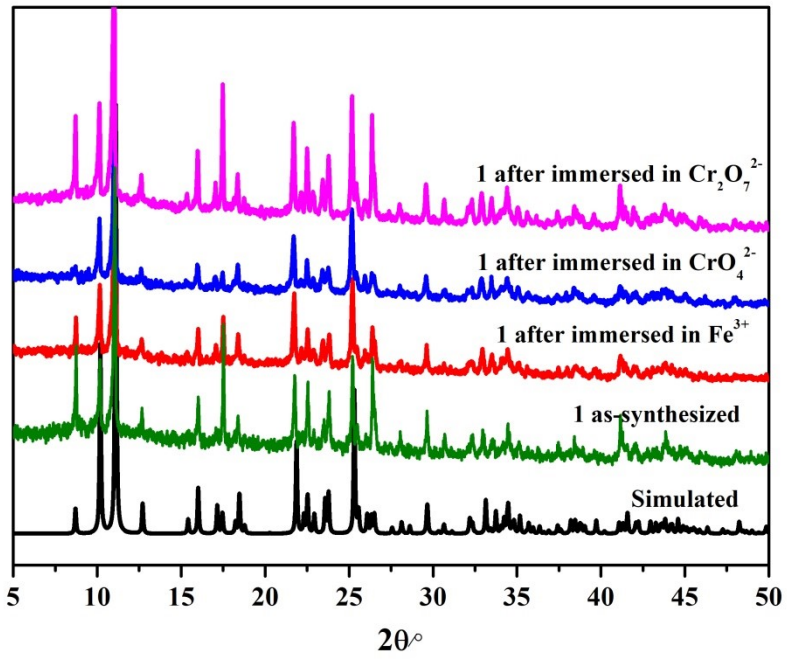

Fig.S9 PXRD patterns for complex **1** and **1** after immersed in Fe^{3+}, $Cr_2O_7^{2-}$, CrO_4^{2-} ions for 72h.

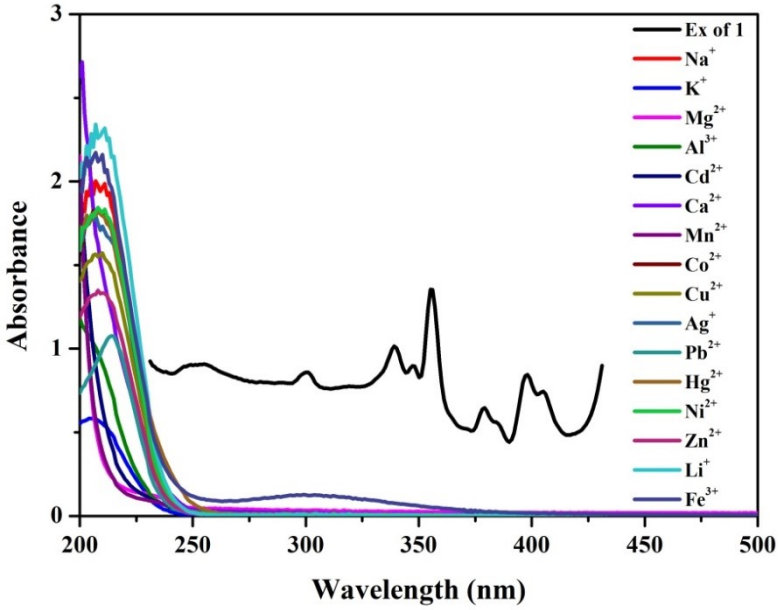

Fig.S10 The UV-Vis adsorption spectra of different metal ions and the excitation spectrum of **1** in aqueous solutions

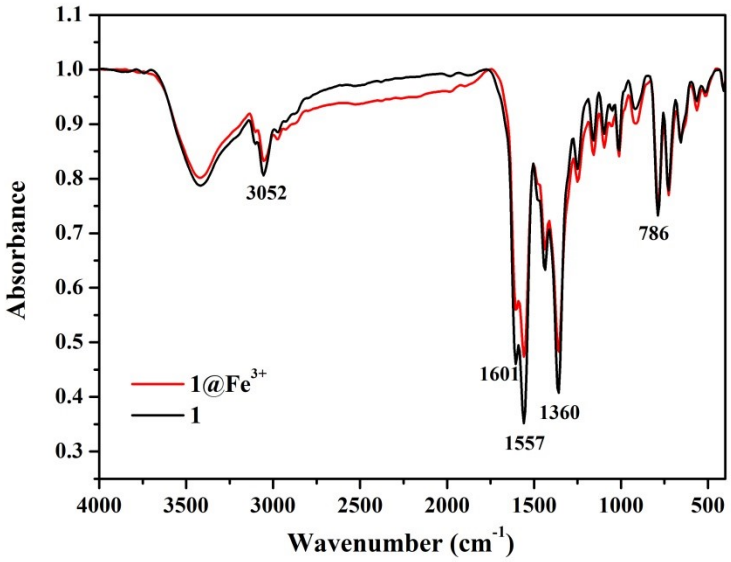

Fig.S11 IR spectra of complex **1** and **1** after immersed in Fe^{3+} ions.

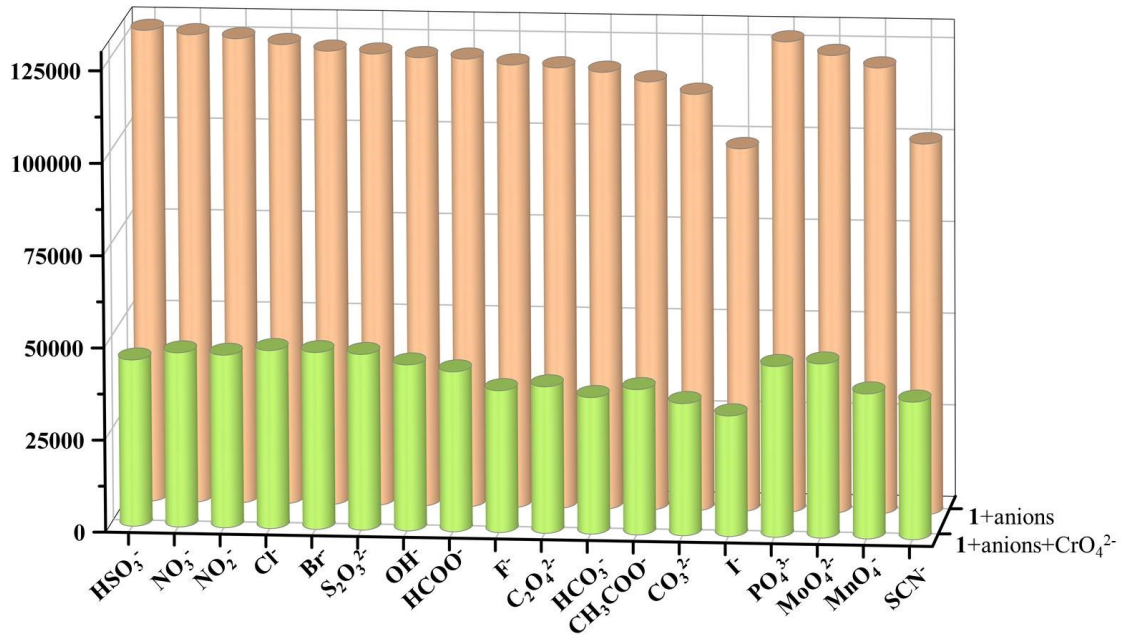

Fig.S12 The anti-interference experiment of complex **1** for detecting CrO_4^{2-} ions in the presence of other anions (1.0×10^{-3} M).

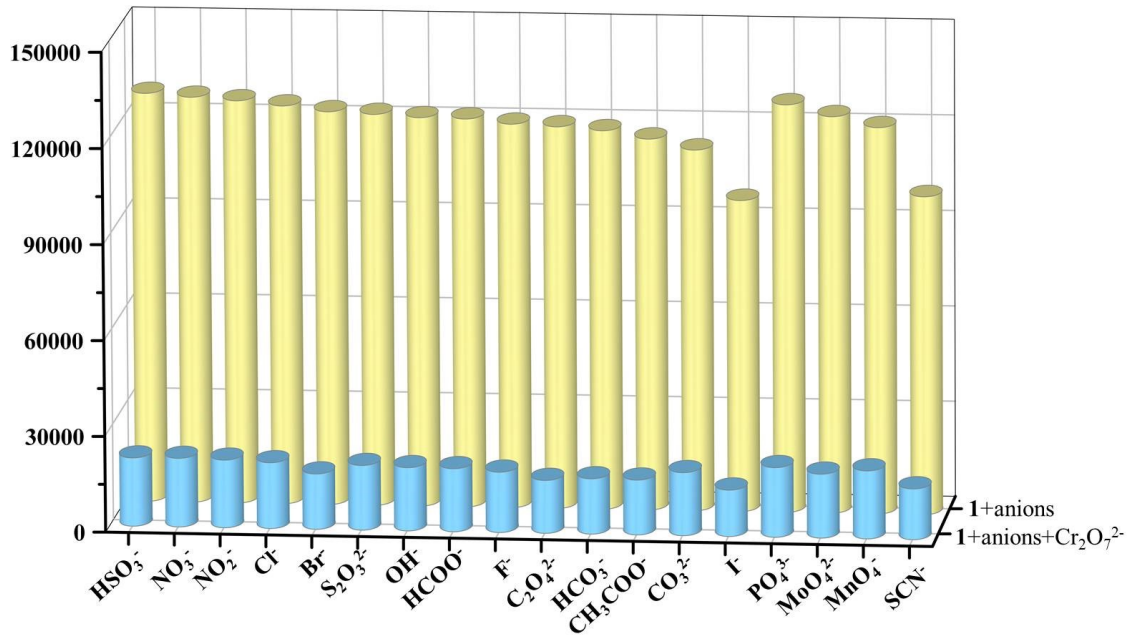

Fig.S13 The anti-interference experiment of complex 1 for detecting $Cr_2O_7^{2-}$ ions in the presence of other anions (1.0×10^{-3} M).

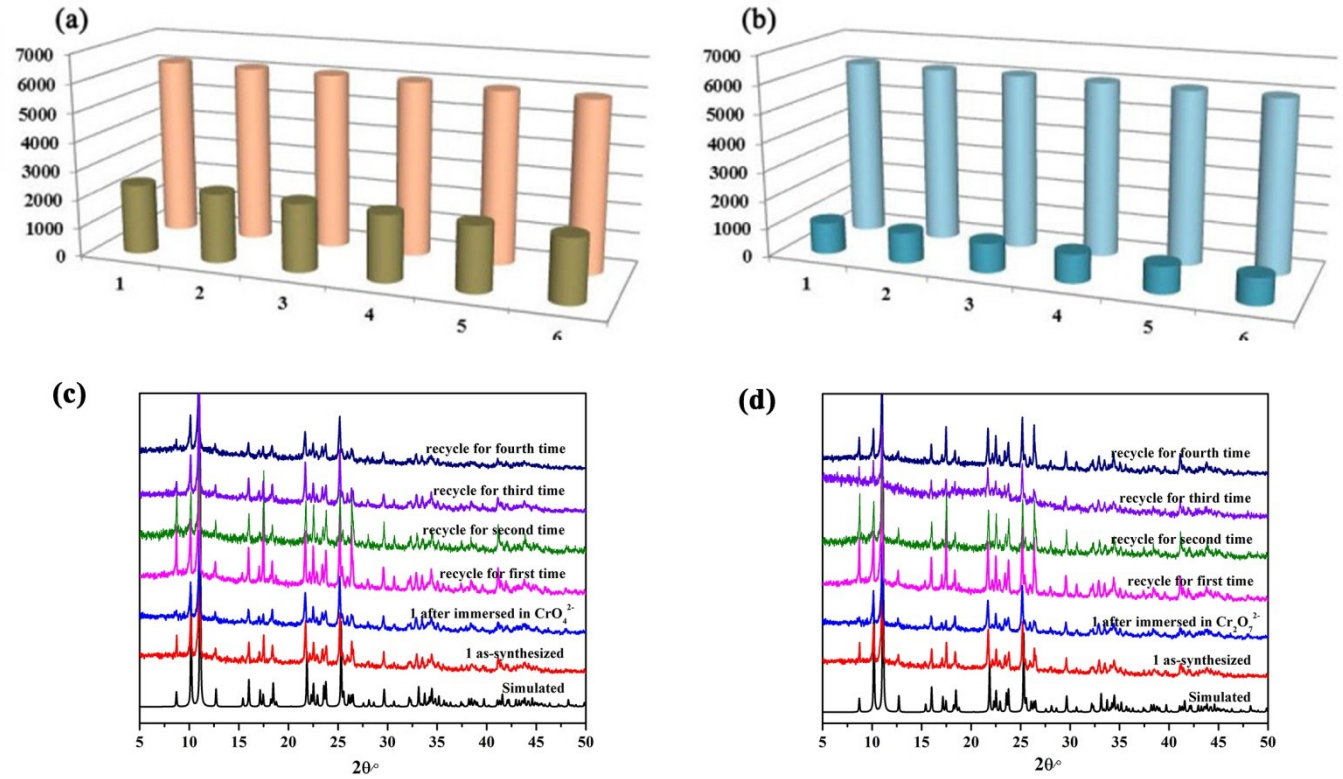

Fig.S14 Recovery experiment of CrO_4^{2-}(a)/ $Cr_2O_7^{2-}$(b) detected by complex **1**: the light colored cylindrical bar represents the initial luminous intensity, and the dark colored cylindrical bar represents the luminous intensity after adding CrO_4^{2-}(a)/ $Cr_2O_7^{2-}$(b) ions; (c) (d) PXRD patterns complex **1** after cycling.

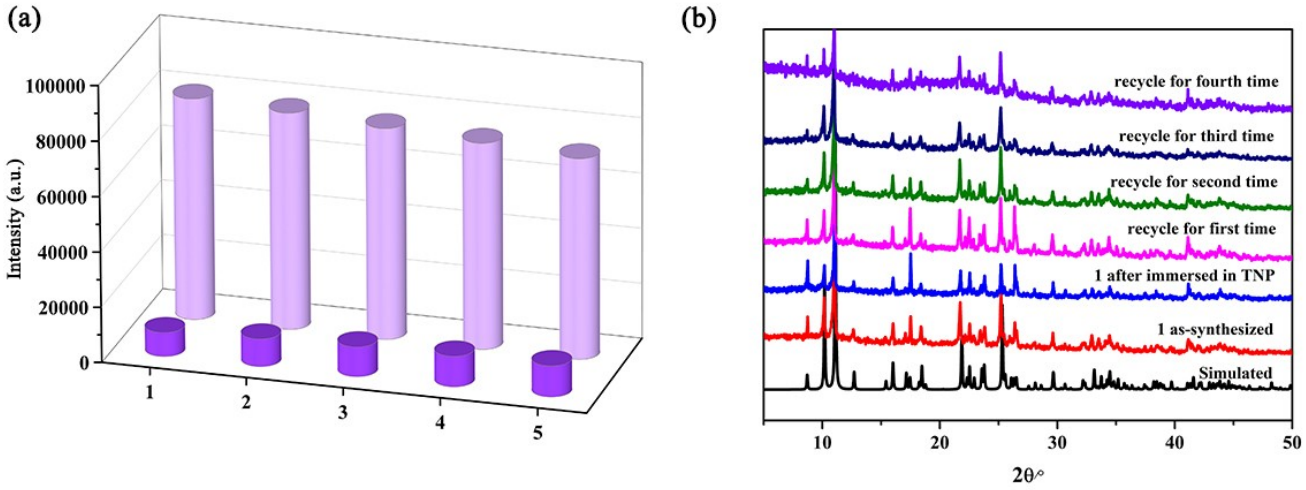

Fig.S15 (a) Recovery experiment of TNP detected by complex **1**: the light colored cylindrical bar represents the initial luminous intensity, and the dark colored cylindrical bar represents the luminous intensity after adding TNP ions; (b) PXRD patterns complex **1** after cycling

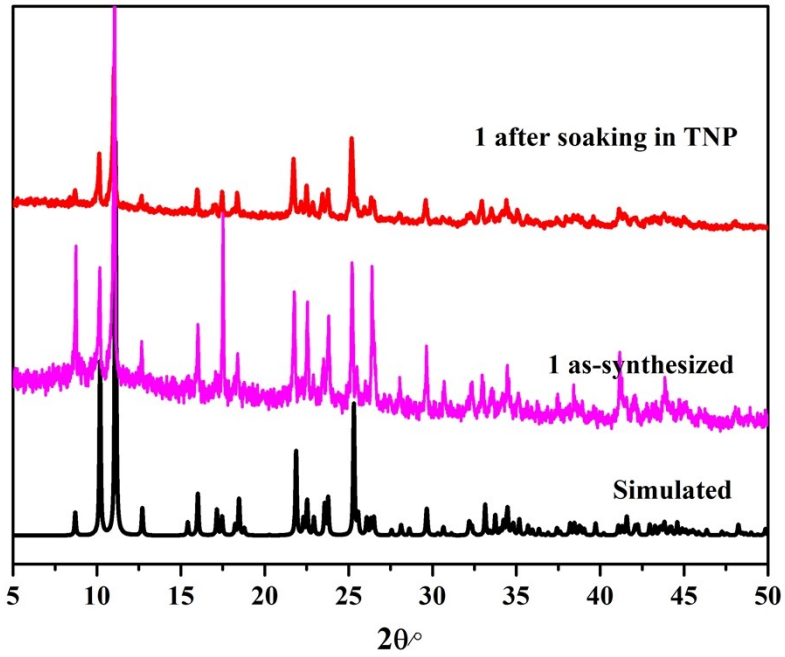

Fig.S16 PXRD for complex **1** and **1** after soaking in TNP solvents for 72h.

Table S1 The BET specific surface area and the pore structure data.

Sample No.	Formula	BET surface area (m^2/g)	Pore volume (cm^3/g)	Average pore diameter (nm)
1	$C_{23}H_{13}N_3O_4Cd$	3.18	0.008	8.86

Table S2 The crystal data for **1**

Compound	**2**
Formula	$C_{23}H_{13}N_3O_4Cd$
Formula weight	507.76
T/K	113
Crystal system	Orthorhombic
Space group	*Fddd*
a(Å)	8.9617(12)
b(Å)	19.198(3)
c(Å)	40.595(7)
α(°)	90.000
β(°)	90.000
γ(°)	90.000
V(Å^3)	6984.5(19)
Z	16
D_{calc}(g cm$^{-3)}$	1.932
μ (mm^{-1})	1.292
F(000)	4032.0
Rint	0.0608
GOOF	1.121
R_1[a] [I > 2σ(I)]	0.0369
ωR_2[b] [I > 2σ(I)]	0.0793
R_1 (all data)	0.0535
wR_2 (all data)	0.0869
largest diff. peak and hole (e Å^{-3})	1.830, -0.997

Table S3 Selected bond lengths [Å] and angles [°] for **1**

Complex **1**			
Cd(1)-O(1)#1	2.273(8)	Cd(1)-O(1)#2	2.273(8)
Cd (1)-N(2)	2.336(10)	Cd (1)-N(1)#3	2.362(8)
Cd (1)-N(1)	2.362(8)	Cd(1)-O(2)#2	2.738(10)
Cd(1)-O(2)#1	2.738(10)		
O(1)#1-Cd(1)-O(1)#2	108.1(4)	O(1)#1-Cd(1)-N(2)	125.9(2)
O(1)#2-Cd(1)-N(2)	125.9(2)	O(1)#1-Cd(1)-N(1)#3	87.0(3)
O(1)#2-Cd(1)-N(1)#3	118.5(3)	N(2)-Cd(1)-N(1)#3	68.7(2)
O(1)#1-Cd(1)-N(1)	118.5(3)	O(1)#2-Cd(1)-N(1)	87.0(3)
N(2)-Cd(1)-N(1)	68.7(2)	N(1)#3-Cd(1)-N(1)	137.5(4)
O(1)#1-Cd(1)-O(2)#2	149.7(3)	O(1)#2-Cd(1)-O(2)#2	49.4(3)
N(2)-Cd(1)-O(2)#2	79.56(16)	N(1)#3-Cd(1)-O(2)#2	88.5(3)
N(1)-Cd(1)-O(2)#2	83.9(3)	O(1)#1-Cd(1)-O(2)#1	49.4(3)
O(1)#2-Cd(1)-O(2)#1	149.7(3)	N(2)-Cd(1)-O(2)#1	79.56(16)
N(1)#3-Cd(1)-O(2)#1	83.9(3)	N(1)-Cd(1)-O(2)#1	88.5(3)
O(2)#2-Cd(1)-O(2)#1	159.1(3)		
Symmetry transformations used to generate equivalent atoms: #1 -x+1,-y,-z+2 #2 -x,-y,-z+2			

Table S4 HOMO and LUMO energies calculated for nitroaromatic explosives at B3LYP/6-31G** level of theory

Analytes	**HOMO (eV)**	**LUMO (eV)**	**Band gap**
TNP [1]	-8.2374	-3.8978	4.3396
TNT [1]	-8.4592	-3.4926	4.9666
1,3-DNB [1]	-7.9855	-3.4311	4.5544
2,4-DNT [1]	-7.7645	-3.2174	4.5471
NB [1]	-7.5912	-2.4283	5.1629
1,4-DNB [2]	-8.3525	-3.4967	4.8557
1,3,5-TNB [2]	-8.9338	-3.6831	5.2507

Table S5 Comparison of literature reports for complexes as sensors of TNP

Complexes	K_{sv} **(M^{-1})**	**Detection Limit**	**Ref.**
$[Cd(dbta)]_n$ (1)	6.24×10^3	5.35×10^{-5} M	**This work**
$\{[La(H_2O)_4(HL)]\cdot H_2O\}$ (1)	4.61×10^4	4.13×10^{-6} M	[3]
(Probe 1) N,N'-(2-hydroxypropane-1,3-diyl)bis(1,8-naphthalimide-m-benzenesulfonamide)	1.35×10^7	5.86 ppt	[4]
$[Zn_2(1,2\text{-bdc})_2(BPDPE)_2]_n$ (1)	1.99×10^4	2.54×10^{-6} M	[5]
$[Zn_2(L^2)(\mu_{1,5}\text{-dca})_2(\mu_1\text{-dca})]_n$ (2)	1.542×10^4	0.0985 ppm	[6]
$[Ba(PSTP)_{0.5}(H_2O)]_n$ (1)	9.6×10^5	0.31 ppm	[7]
DFCAP	4.14×10^5	1.74 μM	[8]
SP	9.74×10^4	19 ppm	[9]
$[(CPh)Al(OH)(H_2O)]NO_3$	/	0.99 μM	[10]
Compound (1)	2.19×10^4	0.79 μM	[11]

References

1. Nagarkar, S. S.; Joarder, B.; Chaudhari, A. K.; Mukherjee, S.; Ghosh, S. K. Highly selective detection of nitro explosives by a luminescent metal-organic framework. *Angew. Chem. Int. Ed. Engl.* **2013,** *52* (10), 2881-5.
2. Zhang, X.; Zhan, Z.; Liang, X.; Chen, C.; Liu, X.; Jia, Y.; Hu, M. Lanthanide-MOFs constructed from mixed dicarboxylate ligands as selective multi-responsive luminescent sensors. *Dalton. Trans.* **2018,** *47* (10), 3272-3282.
3. Wu, M.; Zhang, H.; Ge, C.; Wu, J.; Ma, S.; Yuan, Y.; Zhao, L.; Yao, T.; Zhang, X.; Yang, Q. A stable lanthanum-based metal-organic framework as fluorescent sensor for detecting TNP and Fe(3+) with hyper-sensitivity and ultra-selectivity. *Spectrochim. Acta, Part A.* **2022,** *264*, 120276.
4. Kumar, A.; Chae, P. S. New 1,8-naphthalimide-conjugated sulfonamide probes for TNP sensing in water. *Sens. Actuators, B.* **2017,** *240*, 1-9.
5. Zhang, L.; Hu, J.; Li, J.; Zhang, J. A thermal and pH stable fluorescent coordination polymer for sensing nitro explosives or metal ions with high selectivity and sensitivity in aqueous solution. *J. Lumin.* **2021,** *234*.
6. Majumdar, D.; Dey, S.; Kumari, A.; Pal, T. K.; Bankura, K.; Mishra, D. Dicyanamide-intertwined assembly of two new Zn complexes based on N2O4-type pro-ligand: Synthesis, crystal networks, spectroscopic insights, and selective nitroaromatic turn-off fluorescence sensing. *Spectrochim. Acta, Part A.* **2021,** *254*, 119612.
7. Sun, Y.; Dong, B.-X.; Liu, W.-L. Construction of a new three-dimensional fluorescent probe based on BaII ions and 2,5-bis-(4-carboxy-phenylsulfanyl)-terephthalic acid. *J. Solid State Chem.* **2019,** *278*.
8. Dey, S.; Maity, A.; Shyamal, M.; Das, D.; Maity, S.; Giri, P. K.; Mudi, N.; Samanta, S. S.; Hazra, P.; Misra, A. An antipyrine based fluorescence "turn-on" dual sensor for Zn(2+) and Al(3+) and its selective fluorescence "turn-off" sensing towards 2,4,6-trinitrophenol (TNP) in the aggregated state. *Photochem. Photobiol. Sci.* **2019,** *18* (11), 2717-2729.
9. Saravanan, S.; Ahmad, R.; Kasthuri, S.; Pal, K.; Raviteja, S.; Nagaraaj, P.; Hoogenboom, R.; Nutalapati, V.; Maji, S. Pyrazoloanthrone-functionalized fluorescent copolymer for the detection and rapid analysis of nitroaromatics. *Mater. Chem. Front.* **2021,** *5* (1), 238-248.
10. Purkait, R.; Dey, A.; Dey, S.; Ray, P. P.; Sinha, C. Design of a coumarinyl-picolinoyl hydrazide Schiff base for the fluorescence turn-on–off sequential sensing of Al3+ and nitroaromatics, and electronic device fabrication. *New J. Chem.* **2019,** *43* (37), 14979-14990.
11. Kose, M.; Kırpık, H.; Kose, A. Fluorimetric detections of nitroaromatic explosives by polyaromatic imine conjugates. *J. Mol. Struct.* **2019,** *1185*, 369-378.